JOURNAL OF PROPULSION AND POWER
Vol. 22, No. 2, March–April 2006

Mesoscale Burner Arrays for Gas-Turbine Reheat Applications

S. Lee,* M. Svrcek,† C. F. Edwards,‡ and C. T. Bowman§
Stanford University, Stanford, California 94305-3032

Mesoscale burner arrays allow combustion to be conducted in a distributed fashion at millimeter (meso) scale. At this scale, diffusive processes are fast, such that a number of advantages over conventional combustion can be achieved without giving up the possibility to use fluid inertia to advantage. Because the scale of the reaction zone follows from the scale at which the reactants are mixed, very compact flames result. We expect that this compact, distributed form of combustion can provide not only the opportunity of interturbine reheat, but also the potential for lean premixed or highly vitiated combustion to suppress NOx emissions. As a proof of concept, a 4 × 4 array with burner elements on 5-mm centers has been fabricated in silicon nitride via shape deposition manufacturing. The array was designed to use gaseous fuel (methane) and swirl stabilization. Results including pressure drop, flame stability, temperature distribution in the burnt gas, and NOx emissions are reported for both a fully premixed (mixing before entry) and partially premixed (mixing in the array) configuration. These results demonstrated the degree to which premixed performance can be achieved with this design and pointed to ways in which the array design could be improved over this first-generation unit.

I. Introduction

IMPROVING the efficiency of gas-turbine engines is a significant challenge. Raising the turbine inlet temperature can improve efficiency, but it can also aggravate NO emissions. Raising the pressure ratio can also improve efficiency, but past a critical value this results in reduced specific work. These conflicting effects suggest a need for developing a conceptually different approach to improving gas-turbine engines, that is, modifying the basic engine cycle to circumvent current design tradeoffs. In this paper we focus on one such modification: use of a reheat cycle. In this concept, a reheat combustor is inserted between turbine stages to increase the gas temperature in the secondary turbine before expansion to exit conditions.

Our approach to implementing the reheat cycle is to use highly distributed, millimeter-scale combustion in the reheat burner. This is achieved by use of a mesoscale array, which features burner elements on 5-mm centers, each of which has its own combination of air and fuel inlet, fuel injection, and swirler. The advantage of this concept is that the fuel-air mixing is performed at a scale where molecular mixing is sufficiently fast that very compact (in axial length) yet distributed (over the array) flames can be achieved. Use of these compact flames can allow introduction of an interturbine reheat combustor without a significant increase in overall engine length and with good control over pattern factor. In this paper, we report preliminary results from a first-generation array using a gaseous fuel (methane).

This well-distributed and compact combustion also allows the potential for achieving low NOx emissions. Current NOx reduction efforts are focused on obtaining nearly premixed emission levels using a lean, direct-injection approach. Distributed mesoscale combustion is ideally suited for this purpose. However, as high-temperature material and blade cooling methods are developed, the permissible turbine inlet temperature is increasing. This might make even premixed NOx emission levels unacceptable. We believe that the best way to reduce NOx emissions further is to employ highly vitiated combustion in which the air-fuel mixture is diluted with previously burned gas and oxidized homogeneously over the reaction region. Because of their highly distributed combustion, their control potential, and their near-diffusive mixing scale, we believe that mesoscale arrays can provide an ideal method for implementing this form of NOx control in gas-turbine engines.

This paper reports preliminary efforts to develop a mesoscale burner array for the reheat application by presenting its design, fabrication process, and experimental testing. As a first demonstration to verify the concept, a 4 × 4 array was fabricated because it is the minimum size required to provide mesoflames without dominant edge effects (mainly air entrainment from the surroundings). Because a primary motivation for developing the array is implementation of a reheat-cycle engine, we begin with a thermodynamic analysis of that engine in order to define desirable operating conditions for the array. The important design and fabrication issues of the 4 × 4 burner array are then presented, and finally the performance of our first-generation array operating in both premixed and partially premixed modes is reported.

II. Reheat Cycle Efficiency

The idea of improving gas-turbine performance through the use of reheat is not new. Analysis of the effects of reheat on ideal cycle performance is standard fare in most courses on thermodynamics. What this analysis shows is that, in the absence of other changes, specific work rises but efficiency declines. The reason for the loss in efficiency is that after each stage of heating the working fluid is not expanded through as large a pressure ratio as a simple-cycle engine, and hence the extraction of energy (as work) is diminished.

One way to remedy the situation is to use regeneration. In this case the energy remaining in the waste gases can be recycled for use in heating the postcompressor gases. Because this task would otherwise fall to the combustor, any energy that can be added from the waste-gas stream directly displaces energy that would have to be added in the form of fuel. The result is a more efficient—as well as more powerful—engine. The difficulty with regeneration is that, to date, it has proven to be impractical for use in flight engines because of weight and/or size limitations.

Regeneration is not the only option available to recoup efficiency. Increasing the overall pressure ratio (OPR) of the engine can also give this result. A key tradeoff in choosing the pressure ratio of a simple-cycle engine is the competition between specific work and efficiency. For a given turbine inlet temperature, use of a high pressure ratio leads to high efficiency but less than optimum work. Conversely, use of reheat leads to high specific work but a decline in efficiency. These opposing tendencies suggest that use of the combination of the two—high-pressure ratio and reheat—is the key to obtaining a high-power-density, efficient gas-turbine engine.

Received 24 January 2005; revision received 15 July 2005; accepted for publication 3 August 2005.

*Ph.D. Student, Mechanical Engineering. Student Member AIAA.
†Graduate Student, Mechanical Engineering.
‡Associate Professor, Mechanical Engineering. Member AIAA.
§Professor, Mechanical Engineering. Member AIAA.

To our knowledge, Liu and Sirignano[1,2] were the first to recognize the potential benefits of this approach. Through a series of papers, they explored possible flight-engine configurations including the effect of pressure ratio, bypass ratio, and afterburning. They have also investigated whether there is benefit to using not just one or two interturbine burners, but of attempting to perform the reheat continuously in the turbine itself. They refer to this latter approach as a continuous-turbine burner.

From their work, a number of conclusions can be drawn. The first is that the key advantage of the reheat-cycle engine is likely to be its power density more than its efficiency. Only small, if any, efficiency advantages (decreases in thrust specific fuel consumption) were observed in their work, whereas gains in specific thrust were substantial. The second conclusion is that very high overall pressure ratios are required to achieve maximum benefit. Increased OPR generally increases specific thrust and decreases thrust specific fuel consumption of a reheat-burner engine. The third is that even with significant increase in specific thrust, use of reheat burners in a turbojet at low flight Mach numbers induces low propulsion efficiency. Therefore, the appropriate role for this technology in subsonic flight is most likely to form a high-power-density core for a turbofan engine. The final conclusion is that the performance of the reheat-cycle engine improves with the increase in overall pressure ratio, flight Mach number, and bypass ratio.

We have performed a systematic analysis for a shaft-work producing engine using a single reheat burner to explore the effects such as the overall pressure ratio and the optimum split in pressure ratio between two turbine stages. The calculations use a variable property (specific heat and composition) ideal-gas working fluid and the component performance metrics suggested by Mattingly.[3] These performance metrics are grouped by technology level, indicating the overall state of development of an engine. Mattingly cites four technology levels, ranging from relatively primitive components (level 1) through the most advanced components proposed (level 4). For our purposes, the appropriate technology levels are the best of today (level 3) and those proposed for tomorrow (level 4). Table 1 lists the metrics used in our work for these two levels of technology.

Figure 1 shows the result of a typical calculation on a sensible enthalpy-entropy diagram. Also shown are the process paths for ideal simple-cycle and reheat-cycle operation with the same pressure ratios. The primary conclusion to be drawn from this plot is that the effect of device losses (irreversibilities) is significant. In fact they are sufficiently large that design calculations motivated by ideal-cycle analyses lead to conditions that, with real device efficiencies, are far from their optimum values. Figures 2 and 3 show the performance of simple- and reheat-cycle engines using levels 3 and 4 component efficiencies (respectively) as a function of the overall pressure ratio of the engine. Also shown on these figures is the front pressure ratio (pressure ratio across the first turbine) for peak engine efficiency.

For level 3 components in a simple-cycle engine, we see that the specific work peaks at a pressure ratio near 20, whereas efficiency continues to rise until a pressure ratio of 70 (at which point the specific work has declined by 25%). For the reheat-cycle engine, however, the peak efficiency does not occur until an overall pressure ratio of 100, and the specific work peak occurs at such a low pressure ratio that it is not included on the plot. (Only conditions of acceptable efficiency were computed.) Key features to note are that, at any given overall pressure ratio, the reheat-cycle engine produces 50% more specific work than the simple-cycle engine, and it is not until past a pressure ratio of 80 that the reheat-cycle engine yields

Table 1 Component performance metrices by technology level (after Mattingly[3])

Component	Figure of merit	Level 3	Level 4
Compressor	Polytropic efficiency e_c	88%	90%
Burner	Pressure ratio π_b	0.94	0.95
	Combustion efficiency η_b	98%	99%
Turbine	Polytropic efficiency e_t	87%	89%
	Inlet stagnation temperature T_{t4}	1780 K	2000 K

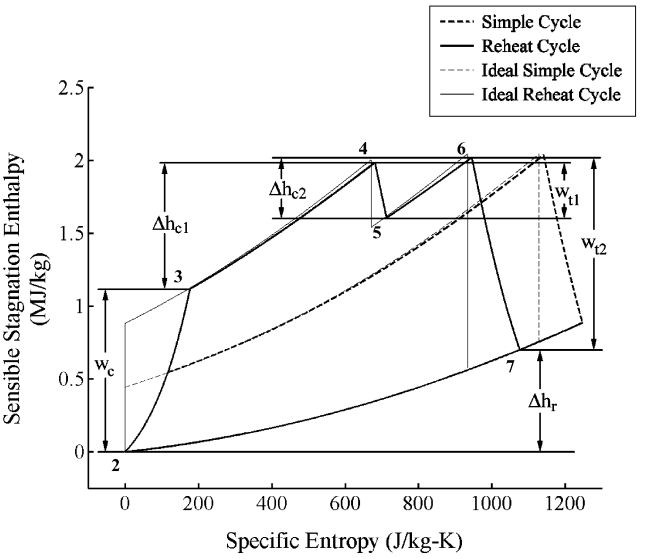

Fig. 1 Sensible stagnation enthalpy vs specific entropy for ideal and level 3 components, simple and reheat cycles.

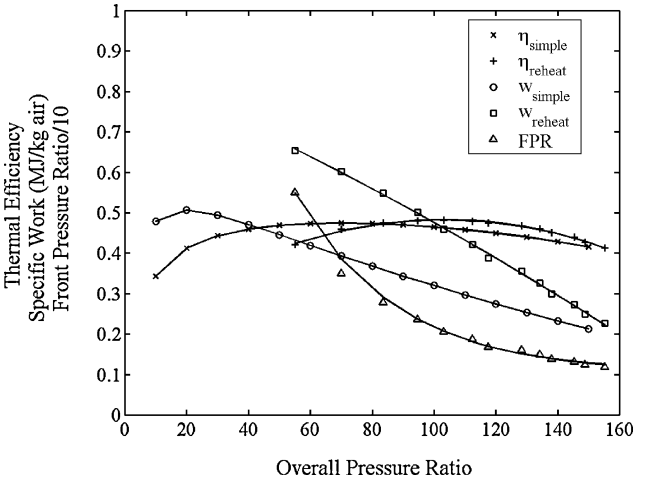

Fig. 2 Specific work and thermal efficiency vs overall pressure ratio for level 3 simple and reheat cycles, with FPR chosen for peak efficiency.

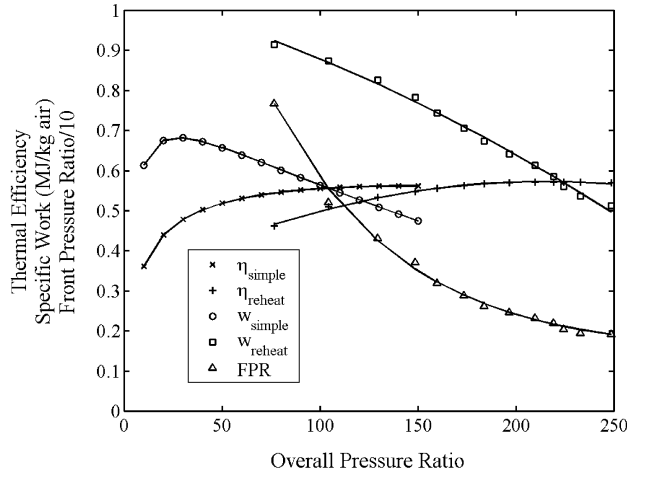

Fig. 3 Specific work and thermal efficiency vs overall pressure ratio for level 4 simple and reheat cycles, with FPR chosen for peak efficiency.

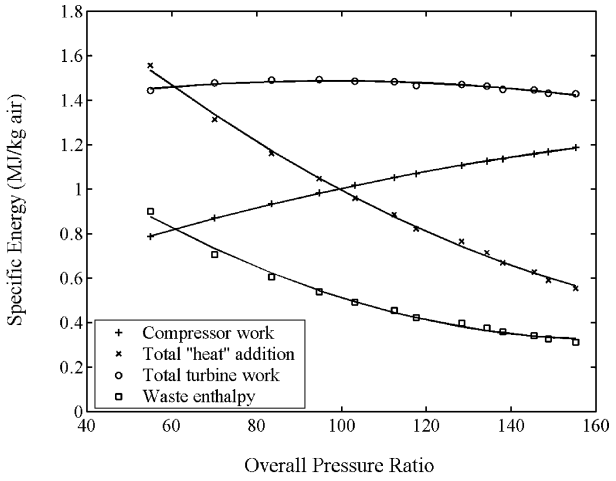

Fig. 4 Energy distribution as a function of overall pressure ratio for a reheat cycle with level 3 components.

a higher efficiency. Also noteworthy is the curve for optimum front pressure ratio: near peak efficiency (OPR∼100), the optimum expansion across the front turbine is ∼2:1, whereas that of the second turbine is ∼50:1.

Figure 3 shows similar results for a level 4 engine. The optimum pressure ratios for specific work and efficiency of the simple-cycle engine have now increased to 30 and 150, respectively. Similarly, the optimum pressure ratio for efficiency in the reheat-cycle engine has now shifted to ∼220, again with a front pressure ratio of ∼2 (and a concomitant back pressure ratio of ∼110). At this technology level, the crossover in efficiency from the simple cycle to the reheat cycle occurs at a pressure ratio of ∼155—again just past the peak of the simple-cycle efficiency. Note too that the specific work of the reheat cycle exceeds that of the simple cycle by ∼30% at any given overall pressure ratio.

A question that naturally arises is the reason for the decline in efficiency past the peak values exhibited in these figures. A plot of the energy distribution between devices (Fig. 4) shows that at high pressure ratios the backwork ratio of the engine becomes large, while the heat addition in the combustors becomes small (because of the temperature cap). The majority of the energy in the system is caught up in cycling through the turbomachinery and is exposed to the inefficiencies of these devices. For this reason, the thermal efficiency rolls off, rather than continuing to increase (as it does for ideal cycles).

Figures 2 and 3 show that for a given overall pressure ratio the reheat-cycle engine always produces a higher level of specific work, and that past a critical pressure ratio efficiency is also improved. But this is not the only comparison that can be made. An equally valid comparison can be made by comparing engines at different overall pressure ratios but equal work or efficiency. Tables 2 and 3 provide these comparisons.

Table 2 shows results for thermal efficiency of the two cycles operated at equal specific work (but different overall pressure ratios). The value of the specific work is chosen in one of three ways: the value of the specific work at its peak for the simple-cycle engine, the value at the peak of efficiency for the simple-cycle engine, and the value at the midpoint pressure ratio (between work and efficiency peaks) of the simple-cycle engine. In each case the operating point of the reheat-cycle engine is chosen to match the specific work of the simple-cycle engine. The results show that for a given specific-work requirement the reheat-cycle engine can provide anywhere from no benefit (<1%) to an 18.6% benefit in efficiency depending upon the choice of operating conditions and technology level.

Table 3 shows the complementary comparison: gain in specific work for the two cycles operating at a fixed level of efficiency. Again the operating points are chosen according to the performance peaks and midpoint tradeoff of the simple-cycle engine. These data show that significant gains in specific work (27–50%) are possible under all conditions.

Table 2 Equal-work comparison of simple and reheat cycles for levels 3 and 4 components at three possible simple-cycle operating conditions[a]

	OPR	BPR, FPR	η_{th}, %	Gain, %
		Peak simple work		
Level 3				
Simple	20	——	41.2	13.8
Reheat	92.6	37.5, 2.47	48.0	
Level 4				
Simple	30	——	47.8	18.6
Reheat	184.1	70, 2.63	56.7	
Ideal (1780 K)				
Simple	30	——	59.1	34.0
Reheat	377.8	128.5, 2.94	78.6	
		Peak simple efficiency		
Level 3				
Simple	70	——	47.4	0.6
Reheat	118.6	70.6, 1.68	47.7	
Level 4				
Simple	150	——	56.2	0.5
Reheat	255.6	136.7, 1.87	56.5	
		Midpoint tradeoff		
Level 3				
Simple	40	——	46.0	5.0
Reheat	101.1	47.2, 2.14	48.3	
Level 4				
Simple	90	——	55.1	3.8
Reheat	219	100, 2.19	57.2	

[a]The pressure ratio split between front and back turbines (FPR, BPR) was chosen for peak efficiency.

Table 3 Equal-efficiency comparison of simple and reheat cycles for levels 3 and 4 components at three possible simple-cycle operating conditions[a]

	OPR	BPR, FPR	w, MJ/kg air	Gain, %
		Peak simple work		
Level 3				
Simple	20	——	0.507	34.7
Reheat	49	8, 6.15	0.683	
Level 4				
Simple	30	——	0.682	33.1
Reheat	85	12.1, 7.02	0.908	
Ideal (1780 K)				
Simple	30	——	0.727	46.1
Reheat	111.4	11, 10.17	1.062	
		Peak simple efficiency		
Level 3				
Simple	70	——	0.394	37.3
Reheat	84.6	29.7, 2.85	0.541	
Level 4				
Simple	150	——	0.475	50.7
Reheat	171.1	58, 2.95	0.716	
		Midpoint tradeoff		
Level 3				
Simple	40	——	0.471	27.8
Reheat	70.2	20, 3.51	0.602	
Level 4				
Simple	90	——	0.582	30.9
Reheat	152.5	44.5, 3.43	0.762	

[a]The pressure ratio split between front and back turbines (FPR, BPR) was chosen for peak efficiency.

The final issue is the influence of combustor pressure drop. This is a critical design parameter because it determines the momentum available to achieve mixing in the combustor. Figure 5 shows the sensitivity of the specific work and thermal efficiency to the fractional drop in stagnation pressure passing through the combustors. (Both combustors experience the same fractional pressure drop.) These results show that gains of ∼4% in work and efficiency (a rise in efficiency from 48 to 50%) are possible by elimination of the assumed 6% pressure drop (the metric for level 3 burners). Given that the gains in efficiency and specific work in moving from a simple cycle to a reheat cycle are 13.8 and 34.7%, respectively, at this operating

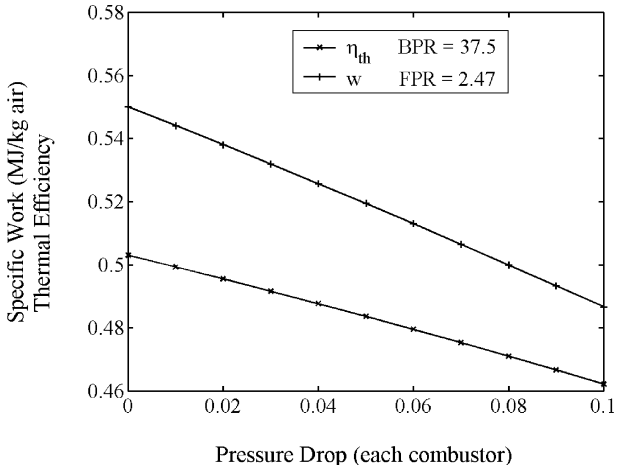

Fig. 5 Rheat-cycle performance as a function of combustor pressure drop for level 3 components. Pressure ratios chosen for equal work at the simple cycle peak-work opertaing condition.

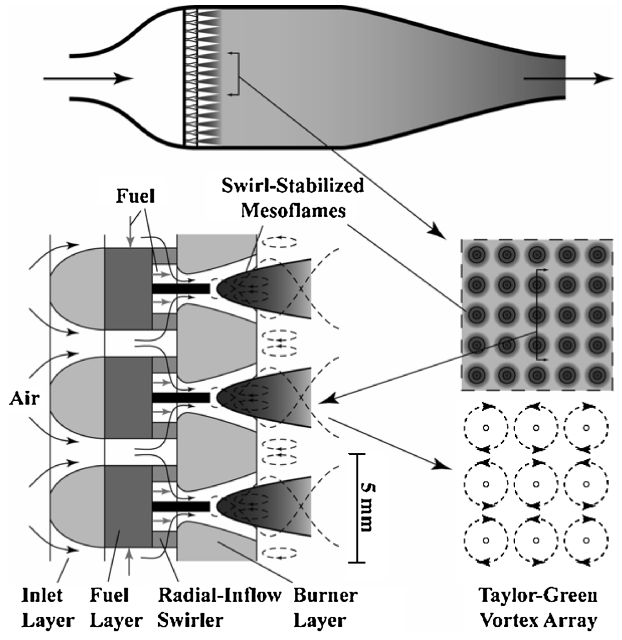

Fig. 6 Basic layout of a three-layer approach to the design of the mesoarray.

point, we believe that it is reasonable to use conventional pressure drops in the combustors as a first step toward implementation of a reheat-cycle engine.

III. Design

The ability to achieve compact, well-distributed flames simplifies interturbine reheat burner design. However, the realization of compact flames in a sufficiently lean or dilute operating range is restricted by flame stabilization. Therefore, achieving effective mixing and diffusion of the reactants and prompt recirculation of burned gases is critical to obtaining flame stability and constitutes a fundamental design challenge. In our present design, swirl was used to induce product recirculation, and a swirl number of unity was selected.

In addition to mixing and stabilization, array pressure drop was included in the design considerations. Values of pressure loss range from 4 to 8% for conventional engines,[4] and so a 6% loss was employed as a design limit. Because the major sources of the loss come from the diffuser, separation in the swirler passages, and drag at the inlet, efforts were made to avoid narrow passages and sudden curvature changes in the airflow path. Although important from a fluid mechanics perspective, these efforts were tempered by manufacturing constraints; our prototype reflects this tradeoff in a number of its features.

The high-temperature environment of the burner element induces a third factor—the material constraint. This was addressed by using silicon nitride (Si_3N_4) for fabrication of the array because of its good combination of thermal properties, corrosion resistance, and mechanical strength at high temperature.

Figure 6 shows the basic design of a three-layer approach that provides an outline for the fundamental design of the array. A three-dimensional CAD image of the prototype mesoburner array as implemented in a single monolithic unit in silicon nitride is also illustrated in Fig. 7. The inlet layer is designed to have streamlined contours to reduce the pressure drop across each burner element. Air enters the burner element in the axial direction in the inlet layer, passes through the fuel layer, and makes a right-angle turn into a radial-inflow swirler. For the fuel layer, gaseous fuel (methane) is injected through an array of four holes at the bottom of the swirler (the top plate of fuel layer) and allowed to mix with the swirling airstream. In future applications, in which we anticipate use of embedded actuators and liquid fuels, all actuation, signal processing, and liquid-handling elements will be implemented in this layer.

Mixing of air with injected fuel, flame stabilization, and combustion occurs downstream of the burner layer. To create a sufficiently large recirculation zone to achieve flame stability, swirl stabilization method is employed using a radial-inflow swirler with two tangential inflows in each burner element. This swirling flow is designed to

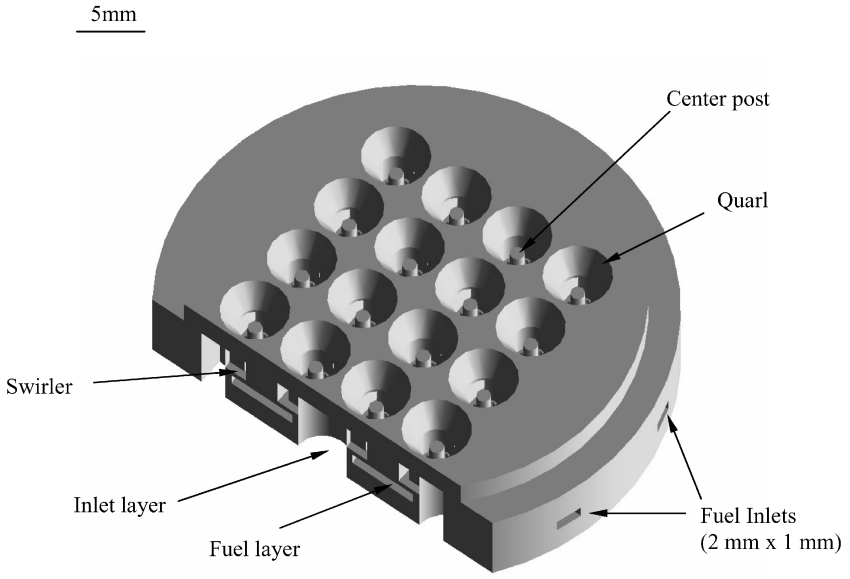

Fig. 7 Angled three-dimensional CAD image of the mesoburner array.

Fig. 8 Prototype 4 × 4 mesoscale burner array fabricated in silicon nitride.

have a counter-rotating circulation pattern (a Taylor–Green vortex array[5]) such that any single flame can propagate over the entire array after ignition. The bluff post at the center of each swirler is also used to improve flame stability. Because a diverging passage downstream of the swirler exit increases both the size of the recirculation zone and the amount of gas recirculated,[4] a diverging quarl is contained in the burner layer. For testing purposes, a circular quartz confinement is used downstream of the array to provide a boundary condition in which there is no free entrainment from the surroundings.

Each of the mesoburners is fabricated by assembly-mold shape deposition manufacturing (SDM) process developed in the Rapid Prototyping Laboratory at Stanford University.[6,7,8] Unlike other rapid prototyping technologies, SDM not only uses layered addition of materials but also subtracts materials, allowing the fabrication of complex parts. Details of the fabrication procedures are presented in another study.[9]

Although the assembly-mold SDM process has several advantages, especially in building very complicated features, there are some difficulties associated with achieving high accuracy. There is the possibility of geometrical inaccuracy during the mold assembly process, which can cause a lack of concentricity or the occurrence of film-shaped burrs (from gaps at the interfaces between the molds). Cracks can also occur if the shrinkage rate during sintering is nonuniform. In the mesoarray fabrication, these inaccuracies affected only the components with very small dimensions (less than 1 mm) such as the fuel plenum and the fuel-injection nozzles. This in turn led to a fuel maldistribution problem in partially premixed operation, as we will show shortly. A picture of the completed prototype array is shown in Fig. 8.

IV. Results

Following completion of the burner array, its performance parameters were measured for both fully and partially premixed (dynamically mixed) operations. The tests with fully premixed gases were conducted to demonstrate the level of performance that could be achieved in this design if complete mixing were achieved.

A. Pressure Drop and Stability

Figure 9 shows an angled view of 16 mesoflames on the array in the partially premixed operating condition. As shown in the figure, compact and well-distributed flames are successfully obtained at lean operating conditions. The flames are, on average, 11–12 mm in length, but small variations exist in the length of individual flames. This is attributed to maldistribution of the fuel between burner elements because of manufacturing tolerances. The fully premixed test shows shorter (8–9 mm), more uniform flames. The longer partially premixed flames suggest that the air and fuel are not sufficiently mixed and that initiation of the reaction is delayed in comparison to the fully premixed case.

Figure 10 shows the pressure drop across the array for a cold-flow test as a function of airflow rate. This pressure drop is incurred because of flow resistance through the array and is defined by $\Delta P = (P_1 - P_2)/P_1$. P_1 is the pressure upstream of the inlet layer

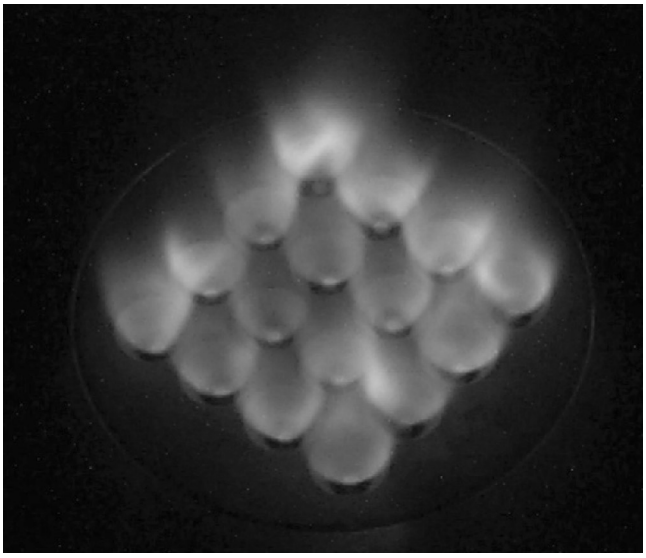

Fig. 9 Self-luminosity photograph of the mesoflames operating under dynamic mixing (partially premixed) conditions at an overall equivalence ratio of 0.8. Compared to the fully premixed conditions, apart from slight luminosity differences between each flame element, there is minimal difference in appearance.

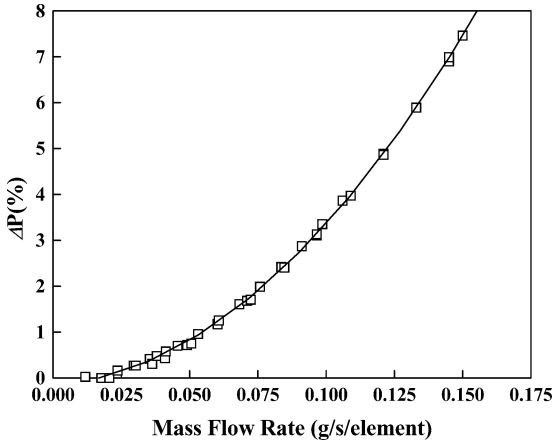

Fig. 10 Pressure drop along the airflow path as a function of mass flow rate. For our target firing rate of 200-W/element, a mass flow rate of 0.14 g/s/element ($\Delta P \sim 6\%$) is required.

in Fig. 6 and is measured using a manometer. P_2 is the pressure measured downstream of the burner layer. For an equivalence ratio of 0.5 and firing rate of 200-W/element (this is the peak power density required in the conventional gas-turbine main burner application; the reheat application requires less power density), a 6.3% pressure loss was measured. This is higher than our initial design point, but acceptable for a first-generation design.

The stability characteristics of the array for both partially and fully premixed conditions are shown in Fig. 11. The stability test was performed by increasing the airflow rate for a fixed firing (fuel) rate. As the amount of air increased, liftoff occurred one by one until all of the flames were lifted from their quarls. This last liftoff point was defined as a blowout point. The plot shows that stable combustion could be sustained down to an equivalence ratio of 0.58 for the fully premixed flames, but at only one-quarter of the design goal of 200 W per element. This means that the recirculation zone was too small, causing blowout prior to the attainment of sufficient residence time to achieve a higher firing rate. Efforts are currently underway to extend the blowout limit of the burner by improving the ratio of residence time to chemical reaction time by creating a larger recirculation zone. The propagation of flames caused by counter-rotating vortices could also be observed during the testing

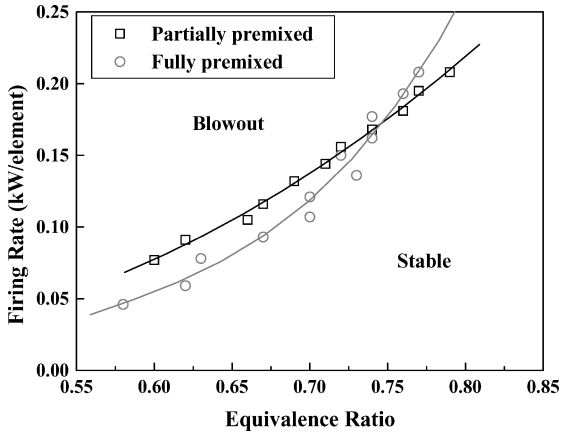

Fig. 11 Flame stability tests for the partially premixed and fully premixed cases.

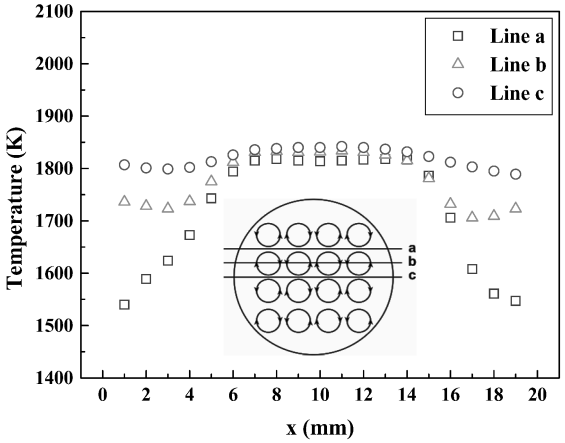

Fig. 12 Temperature distribution at an overall equivalence ratio of 0.68 and firing rate of 47-W/element for fully premixed conditions.

when the operating point was transitioned from near the blowout limit to a more stable region. In each case, the remaining solitary flame was able to relight all of the other burners through cross-burner flow interaction.

We believe that the difference in stability characteristics between the fully and partially premixed cases shown in Fig. 11 is mainly caused by fuel maldistribution in the partially premixed case. Because of the uneven distribution of fuel-produced element-to-element variations in equivalence ratio, some burner elements are richer than others and resist liftoff, while leaner elements lift more easily. This resulted in a better last liftoff but a worse first liftoff characteristic than for the fully premixed case as such infinitely fast mixing might not always be desirable.

B. Temperature Measurements

Temperature distributions for both partially and fully premixed operating conditions were measured using an R-type thermocouple with a 0.254-mm bead. These temperature measurements are performed not only to evaluate the performance of the array, but also to confirm the NO measurements in the following section because NO formation is a strong function of temperature.

Figure 12 shows the spatial variation (x coordinate) of temperature at an axial distance (z), which is 20 mm from the exit plane of the array. Three transverse sweeps are shown, along the lines denoted a, b, and c in the graphic insert. The data show that the counter-rotating vortex pattern results in significantly different temperature depending upon where the measurements are performed. Along line c the gases flow outward from the high-temperature center of the array, resulting in a high temperature and slight gradient at the boundary. Conversely, along line a the effect of entrainment

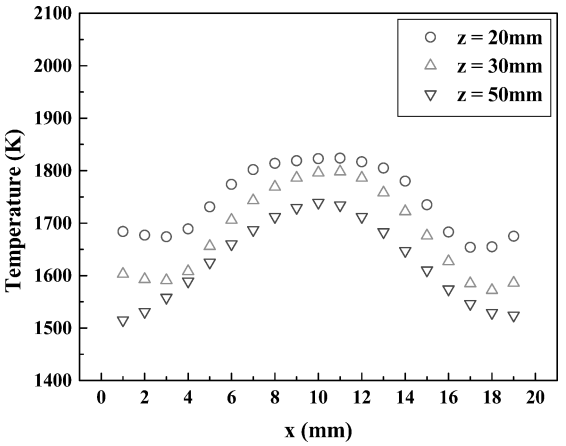

Fig. 13 Tempereture distribution along line b as a function of axial position above the burner face for fully premixed conditions (equivalence ratio 0.68, firing rate 47-W/element).

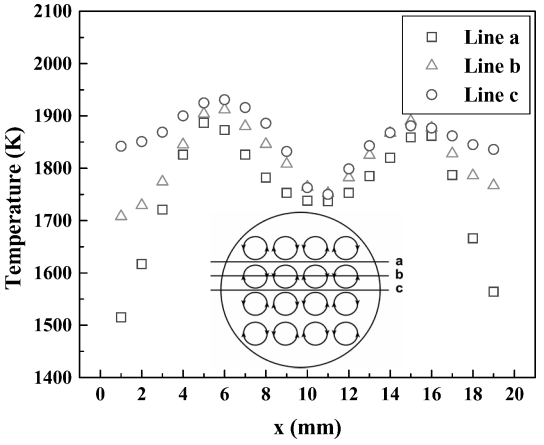

Fig. 14 Temperature distribution at an overall equivalence ratio of 0.68 and firing rate of 47-W/element for partially premixed conditions.

of the relatively cool recirculation products can be seen. However, despite this entrainment, the temperature distribution at the center of the array remains uniform. This is the reason that a 4×4 array was chosen as the minimum scale for testing—it was thought that perhaps the center four elements might be sufficiently isolated from edge effects to provide data representative of a larger array. Figure 13 shows the temperature distribution along line b at various axial locations. As expected, the combined effects of cold entrainment from the surrounding and heat loss to the boundary are increased as the combustion gas travels upward, exhibiting an overall decrease in temperature.

The corresponding temperature measurements under partially premixed conditions are shown in Figs. 14 and 15. In contrast to the fully premixed case, Fig. 14 shows a large variation of temperature with transverse position along the lines. We believe that this temperature variation is mainly caused by two effects; entrainment from the surroundings and element-to-element variations in equivalence ratio. The effects of cold entrainment from the surroundings can be observed by the trailing temperatures at the edges of the burner in Fig. 14. The element-to-element variations in the equivalence ratio are evidenced by the temperature dip near the center of the burner. The two peaks in temperature are actually higher than the adiabatic flame temperature of an overall equivalence ratio of 0.68, indicating that the edge elements are richer than the center elements. In Fig. 15, we can see that the two peaks in the temperature migrate towards each other and merge with rising measurement location. Once again, the effects of air entrainment and heat loss to the boundary are evident in the figure.

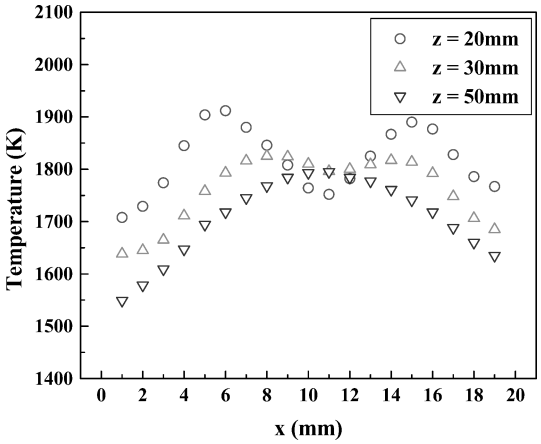

Fig. 15 Temperature distribution along line *b* as a function of axial position above the burner face for partially premixed conditions (equivalence ratio 0.68, firing rate 47-W/element).

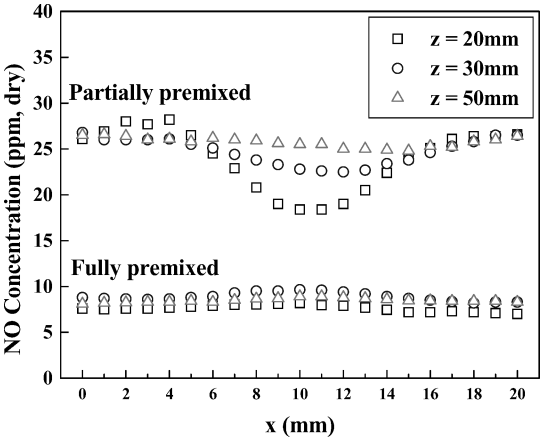

Fig. 16 NO distribution along line *b* for both partially premixed and fully premixed cases as a function of axial position (equivalence ratio 0.68, firing rate 47-W/element).

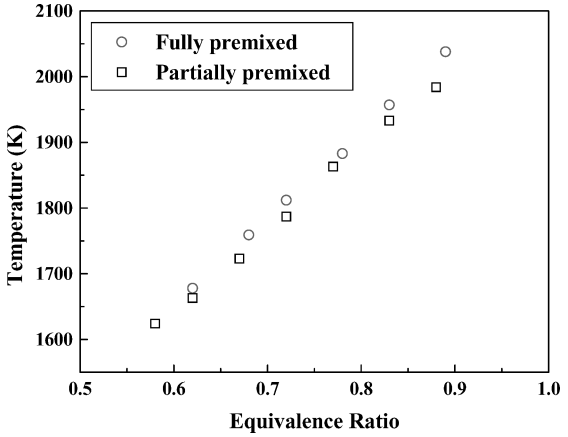

Fig. 17 Temperature vs equivalence ratio under mixed-out conditions ($x = 0$, $z = 60$ mm) for both partially premixed and fully premixed cases at a firing rate of 47-W/element.

C. NO Concentration Measurements

Nitric-oxide emission measurements were made using a chemiluminescent analyzer. All measurements were made using an uncooled near-isokinetic sampling probed inserted from the downstream direction and are reported on a dry basis.

Figure 16 shows the axial variations of the NO concentration in both test conditions as a function of x along line b. As expected from the temperature measurements, a large variation of NO concentration is observed for partially premixed operation, whereas low

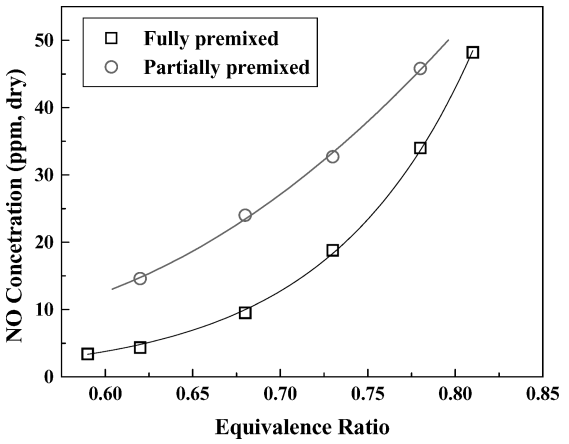

Fig. 18 NO emission vs equivalence ratio under mixed-out conditions ($x = 0$, $z = 60$ mm) for both partially premixed and fully premixed cases at a firing rate of 47-W/element.

and uniform distribution of NO concentration is measured for the fully premixed condition. Unlike temperature, however, NO emissions are not decreased near the boundary for both conditions at $z = 20$ mm. We believe that this is because most of the NO is formed at the flame front, which is short and therefore is well before the region where cold-air entrainment from the surroundings becomes significant. In addition, it is observed that about four times more NO was produced in the partially premixed flames. This confirms that the degree of mixing of fuel and air achieved in the design did not reach the homogeneous level and that better mixing performance is needed for the design to achieve its full potential.

Mixed-out values ($x = 0$, $z = 60$ mm) of temperature and NO are shown as functions of overall equivalence ratio in Figs. 17 and 18. Not surprisingly, as equivalence ratio increases, both temperature and NO concentration are also observed to increase.

V. Conclusions

This paper presented the development efforts of a mesoscale burner array for an interturbine reheat combustor application. A 4×4 ceramic burner array was built by assembly-mold SDM and served as the first demonstration of the compact and well-distributed flames. The array was tested in order to evaluate its various performance parameters, and its results suggest the directions for further improvements. From the work, the following specific conclusions can be drawn:

1) Thermodynamic modeling indicates that use of interturbine reheat while operating at a high overall pressure ratio could improve thermal efficiency by as much as 16% (for equal work) or improve specific work by as much as 38% (for equal efficiency).

2) Mesoscale burner arrays suitable for use in gas-turbine combustion can be successfully fabricated in silicon nitride and operated over a range of firing conditions.

3) The peak firing rate of the first-generation design is of the same order as that required to match peak heat-release rates of current gas-turbine engines. The corresponding pressure drop at this condition is $\sim$6%.

4) Counter-rotating vortex pattern induces cold entrainment to the boundary burner elements so that the temperature near the edges is decreased.

5) In partially premixed operating conditions, element-to-element variations in equivalence ratio are caused by fuel maldistribution, which subsequently influences various performance parameters such as temperature, NO emission, and stability of the burner array.

6) Operation of the array under fully premixed conditions indicates that further improvements in air/fuel mixing (and therefore NO emissions) are possible.

Efforts are currently underway to improve the performance of the mesoscale burner array. The work for the next-generation design is

focusing on improving the degree of mixing toward the premixed level and increasing the strength of the recirculation zone to achieve higher firing rates at lean operating conditions. In addition, a design for use of liquid fuels and suitable for operation at reheat temperature and pressure is also being developed.

Appendix: Thermodynamic of Analysis

Zero-dimensional thermodynamic-cycle analysis for an engine using a single reheat burner between two turbine stages was performed in order to define desirable operating ranges for the array. Both variations of specific heat with temperature and fuel/air ratio and component loss, which is described through the use of isentropic efficiencies, are used to achieve a realistic analysis. As in the simple cycle, it is assumed in the reheat cycle that the working fluid is an ideal gas and all components are well modeled as being adiabatic. Jet A was chosen as a fuel, and standard gas-turbine numbering has been used for each state.[3]

The analysis begins with atmospheric air at state 2 in the reheat cycle diagram of Fig. 1. For the compression process 2–3, the polytropic efficiency of compression e_c is defined by

$$e_c = \frac{\mathrm{d}h_{ts}}{\mathrm{d}h_t} = \frac{\mathrm{d}T_{ts}}{\mathrm{d}T_t} \tag{A1}$$

where t and s denote stagnation state and isentropic process, respectively. For an isentropic process, we have

$$\mathrm{d}T_{ts} = T_t\left\{[(P_t + \mathrm{d}P_{ts})/P_t]^{(\gamma-1)/\gamma} - 1\right\} \tag{A2}$$

The actual and isentropic pressures are identical, and therefore using the binomial expansion for $\mathrm{d}P_t/P_t \ll 1$ results in[10]

$$(1 + \mathrm{d}P_t/P_t)^{(\gamma-1)/\gamma} = 1 + [(\gamma-1)/\gamma](\mathrm{d}P_t/P_t) \tag{A3}$$

By combining Eqs. (A1–A3), the relationship between T_t and P_t in the compressor is obtained as follows:

$$\mathrm{d}T_t/T_t = [(\gamma-1)/\gamma e_c](\mathrm{d}P_t/P_t) \tag{A4}$$

The compressor exit pressure P_{t3} can easily be determined from a given OPR. With this P_{t3}, Eq. (A4) was used to obtain the compressor exit temperature T_{t3} and the specific entropy and sensible stagnation enthalpy changes during compression. In the main combustor, the fuel is mixed with the air, and combustion occurs. Therefore, the effects of a fluid composition change on specific heat were implemented in the analysis. Combustion efficiency η_b and pressure ratio π_b in Table 1 were used to calculate amount of heat addition Q_b, burner exit pressure P_{t4}, and entropy increase during combustion process as follows:

$$Q_b = \eta_b \dot{m}_f Q_f \tag{A5}$$

$$P_{t4} = \pi_b P_{t3} \tag{A6}$$

where $\dot{m}_f$ stands for the total fuel mass flow rate and Q_f is the heating value of the fuel. In solving Eq. (A5), the fuel flow rate was determined by the amount of heat addition, which is limited by the turbine inlet temperature T_{t4}.

The exit pressure of the first turbine P_{t5} can be calculated from the front pressure ratio. The relationship between T_t and P_t for each turbine stage is obtained from the definition of the polytropic efficiency of expansion e_t, and Eqs. (A2) and (A3) as follows:

$$e_t = \frac{\mathrm{d}h_t}{\mathrm{d}h_{ts}} = \frac{\mathrm{d}T_t}{\mathrm{d}T_{ts}} \tag{A7}$$

$$\frac{\mathrm{d}T_t}{T_t} = \frac{e_t(\gamma-1)}{\gamma}\frac{\mathrm{d}P_t}{P_t} \tag{A8}$$

As in the compression process, Eq. (A8) and the exit pressures of the first and second turbines (P_{t5} and P_{t7}) are used to estimate the exit temperatures (T_{t5} and T_{t7}) and the specific entropy and sensible stagnation enthalpy changes. The process 5–6 in Fig. 1 shows a single reheat combustor in between expansion processes. The same equations and component loss are applied to the reheat burner as the main burner except the fact that they have different initial and final states.

Because the specific heat of working fluid varies with temperature and composition, the set of equations just outlined is solved numerically for each state. After obtaining the properties at each state, specific work determined from an energy balance and thermal efficiency η_t is calculated and plotted in terms of OPR.

Acknowledgments

The authors thank NASA for its support under the Ultra-Efficient Engine Technology Program, Grant NAG2-1219. The grant manager is Nagi Mansour.

Discussions on the fabrication of silicon nitride parts with S. Kang, F. B. Prinz, and their colleagues at Stanford Rapid Prototyping Laboratory have been very helpful.

References

[1]Liu, F., and Sirignano, W. A., "Turbojet and Turbofan Engine Performance Increases Through Turbine Burners," *Journal of Propulsion and Power*, Vol. 17, No. 3, 2001, pp. 695–705.

[2]Sirignano, W. A., and Liu, F., "Performance Increases for Gas-Turbine Engines Through Combustion Inside the Turbine," *Journal of Propulsion and Power*, Vol. 15, No. 1, 1999, pp. 111–118.

[3]Mattingly, J. D., *Elements of Gas Turbine Propulsion*, 1st ed., McGraw–Hill, New York, 1996.

[4]Lefebvre, A. H., *Gas Turbine Combustion*, 2nd ed., Taylor and Francis, Philadelphia, 1998.

[5]Taylor, G. I., and Green, A. E., "Mechanism of the Production of Small Eddies from Large Ones," *Proceedings of the Royal Society of London, Series A, Mathematical and Physical Sciences*, Vol. 158, No. 895, 1937, pp. 499–521.

[6]Kang, S., "Fabrication of Functional Mesoscopic Ceramic Parts for Micro Gas Turbine Engines," Ph.D. Dissertation, Mechanical Engineering Dept., Stanford Univ., Stanford, CA, Nov. 2001.

[7]Janney, M. A., Ren, W., Kirby, G. H., Nunn, S. D., and Viswanathan, S., "Gelcasting Tooling: Net Shape Ceramic and Green Machining," *Materials and Manufacturing Processes*, Vol. 13, No. 3, 1998, pp. 389–403.

[8]Reed, J. S., *Principles of Ceramic Processing*, 2nd ed., Wiley, New York, 1995.

[9]Liu, H., Lee, S., Kang, S., Edwards, C. F., and Prinz, F. B., "RP of Si3N4 Burner Arrays via Assembly Mould SDM," *Rapid Prototyping Journal*, Vol. 10, No. 4, 2004, pp. 239–246.

[10]Hill, P. G., and Peterson, C. R., *Mechanics and Thermodynamics of Propulsion*, 2nd ed., Addison Wesley, Reading, MA, 1992.